



Article

# Structural and Phase Analysis of the Ausferritic Ductile Cast Iron Matrix Obtained by Heat Treatment and in the Raw State

Leszek Klimek <sup>1</sup>, Grzegorz Gumienny <sup>2,\*</sup>, Bartłomiej Januszewicz <sup>1</sup>, Radomir Atraszkiewicz <sup>1</sup>  
and Katarzyna Buczkowska <sup>3</sup>

<sup>1</sup> Institute of Materials Engineering, Faculty of Mechanical Engineering, Lodz University of Technology, 90-537 Lodz, Poland; leszek.klimek@p.lodz.pl (L.K.); bartlomiej.januszewicz@p.lodz.pl (B.J.); radomir.atraszkiewicz@p.lodz.pl (R.A.)

<sup>2</sup> Department of Materials Engineering and Production Systems, Faculty of Mechanical Engineering, Lodz University of Technology, 90-537 Lodz, Poland

<sup>3</sup> Department of Materials Science, Faculty of Mechanical Engineering, Technical University of Liberec, 461 17 Liberec, Czech Republic; katarzyna.ewa.buczkowska@tul.cz

\* Correspondence: grzegorz.gumienny@p.lodz.pl

**Abstract:** This paper presents a comparative analysis of ausferritic ductile cast iron matrix obtained through heat treatment and in its raw state. Ausferrite without heat treatment was achieved by modifying the chemical composition, while nodular graphite was produced using Inmold technology. The presence of compacted graphite in the as-cast ausferritic cast iron was attributed to elements that impede the crystallization of nodular graphite. This study demonstrates that an ausferritic matrix in ductile cast iron can be achieved by incorporating molybdenum in conjunction with nickel or copper. Thermal and derivative analysis (TDA) revealed a minor thermal effect during the transformation of austenite into bainitic ferrite in as-cast ausferritic cast iron. Furthermore, the transformation of austenite in cast iron containing nickel was observed to occur at a temperature of approximately 60 °C higher than in cast iron with copper. The structure of bainitic ferrite platelets in as-cast ausferritic ductile cast iron resembled that of Austempered Ductile Iron (ADI). It was revealed that the amount of austenite in as-cast ausferritic ductile cast iron is more than double that in ADI. The carbon content of austenite was estimated theoretically, revealing that alloying additives in the as-cast ausferritic ductile cast iron reduce the solubility of carbon in austenite, thereby significantly influencing the properties of the cast iron.

**Keywords:** ductile cast iron; ausferrite; austenite; austempering; Austempered Ductile Iron



**Citation:** Klimek, L.; Gumienny, G.; Januszewicz, B.; Atraszkiewicz, R.; Buczkowska, K. Structural and Phase Analysis of the Ausferritic Ductile Cast Iron Matrix Obtained by Heat Treatment and in the Raw State. *C* **2024**, *10*, 45. <https://doi.org/10.3390/c10020045>

Academic Editor: Stefano Bellucci

Received: 8 April 2024

Revised: 29 April 2024

Accepted: 6 May 2024

Published: 14 May 2024



**Copyright:** © 2024 by the authors. Licensee MDPI, Basel, Switzerland. This article is an open access article distributed under the terms and conditions of the Creative Commons Attribution (CC BY) license (<https://creativecommons.org/licenses/by/4.0/>).

## 1. Introduction

Cast iron is an alloy of iron with carbon and other elements, and its crystallization occurs through eutectic transformation. The basic elements in cast iron are C, Si, and Mn, making it the most used alloy for castings globally. When the eutectic transformation follows the stable system, graphite precipitates form within the microstructure of cast iron. The fundamental shapes of graphite precipitates are outlined in EN ISO 945-1:2019-09 [1].

Cast iron with nodular graphite is considered one of the modern engineering materials with significant application potential. Within its microstructure, there are nodular graphite precipitations with a V or VI shape as defined by EN ISO 945-1:2019-09.

To achieve nodular graphite, specific conditions must be met, including high surface tension at the graphite embryo–liquid interface, low sulfur concentration (less than 0.01%), and oxygen content below 150 ppm. Magnesium is commonly utilized to fulfill these requirements.

The production of nodular cast iron involves several essential technological steps as follows:

1. Melting of cast iron: The chemical composition should be close to eutectic or hypereutectic.

2. Desulfurization of cast iron: Calcium carbide ( $\text{CaC}_2$ ) is a prevalent compound used for desulfurization, aiming for a sulfur content below 0.02%, preferably less than 0.01%, to ensure the nodular graphite shape.
3. Magnesium treatment process: This step involves adding magnesium to cast iron often in the form of an alloy with elements like silicon, calcium, or aluminum (referred to as a master alloy). The low boiling point of magnesium (1107 °C) compared to the temperature of liquid cast iron poses technological challenges, such as metal splashing, pyrotechnic effects, and smoke. Various methods have been developed to address these issues, including ladle methods, cored wire processes, and Inmold techniques.
4. Inoculation: As-cast iron crystallizes in a metastable system post-magnesium treatment, inoculation with ferro-silicon containing simple inoculants is conducted to refine the microstructure.

Table 1 presents the mechanical properties and matrix microstructure of nodular cast iron.

**Table 1.** The mechanical properties and matrix microstructure of ductile cast iron according to EN 1563:2018-10 [2].

Designation	Yield Strength	Tensile Strength	Elongation	Hardness
	$R_{p0.2}$ MPa min.	$R_m$ MPa min.	A * % min.	HBW **
EN-GJS-350-22	220	350	22	less than 160
EN-GJS-400-18	250	400	18	130–175
EN-GJS-400-15	250	400	15	135–180
EN-GJS-450-10	310	450	10	170–200
EN-GJS-500-7	320	500	7	160–210
EN-GJS-600-3	370	600	3	190–270
EN-GJS-700-2	420	700	2	225–305
EN-GJS-800-2	480	800	2	245–335
EN-GJS-900-2	600	900	2	270–360

\*—given for castings with wall thickness  $t \leq 30$  mm. \*\*—given for castings with wall thickness  $t \leq 60$  mm.

Due to increasing customer demands, new types of ductile cast iron with enhanced mechanical properties are currently under development. One notable example is Austempered Ductile Iron (ADI), a form of ductile cast iron strengthened through an isothermal transformation, which has been utilized since 1972 [3]. The matrix of ADI comprises a blend of high-carbon austenite and bainitic ferrite, known as ausferrite [4–18]. This matrix is achieved through a heat treatment process involving austenitization (~900–950 °C) followed by quenching and isothermal holding (~250–400 °C).

The initial treatment duration must be sufficient to facilitate the transformation of matrix components into austenite. Therefore, the most favorable microstructure of a nodular cast iron matrix for producing ausferrite is pearlite, as it offers the shortest paths for carbon atom diffusion. Once the cast iron matrix is fully austenitic, it is removed from the furnace and transferred to a medium at approximately 250–400 °C. Environmentally harmful molten salts are used for isothermal holding. Swift cooling of the cast between the austenitization and the isothermal holding temperatures allows for bypassing the temperature range of the austenite → pearlite transformation. Consequently, overcooled austenite is formed at the bainitic transformation temperature, leading to a partial conversion into lamellar bainitic ferrite. Increasing the temperature of isothermal transformation results in a higher proportion of austenite (up to 40%) and reduced tensile strength. The resulting mixture of ferrite and high-carbon austenite is termed upper ausferrite. Lowering the isothermal holding temperature decreases the amount of austenite and enhances the tensile strength. Bainitic ferrite plates exhibit a more regular shape, characterizing this form of ausferrite as lower ausferrite. The duration of isothermal holding should be carefully selected to

prevent carbide precipitation. Following a well-executed thermal treatment, ADI castings are obtained. The grades of ADI as per EN 1564:2012 [19] are detailed in Table 2.

**Table 2.** Mechanical properties of ADI according to EN 1564:2012.

Designation	Yield Strength	Tensile Strength	Elongation	Hardness
	$R_{p0.2}$ MPa min.	$R_m$ MPa min.	$A$ % min.	HBW
EN-GJS-800-10	500	800	10	250–310
EN-GJS-800-10-RT				
EN-GJS-900-8	600	900	8	280–340
EN-GJS-1050-6	700	1050	6	320–380
EN-GJS-1200-3	850	1200	3	340–420
EN-GJS-1400-1	1100	1400	1	380–480
EN-GJS-800-10	500	800	10	250–310
EN-GJS-800-10-RT				

EN 1564:2012 also provides for two grades of wear-resistant cast iron with increased hardness. They are shown in Table 3.

**Table 3.** Mechanical properties of wear-resistant ADI according to EN 1564:2012.

Designation	Yield Strength	Tensile Strength	Elongation	Hardness
	$R_{p0.2}$ MPa min.	$R_m$ MPa min.	$A$ % min.	HBW min.
EN-GJS-HB400	1100	1400	1	400
EN-GJS-HB450	1300	1600	-	450

Due to its unique properties, ADI is commonly used on machine elements operating under abrasive wear conditions [20–23]. For instance, it finds applications in automotive components, such as camshafts and cam followers, agricultural machinery, like rippers, plow points, wear plates, and harvesters, as well as construction and mining equipment, including digger teeth, cutters, mill hammers, and covers. Additionally, ADI is employed in general industrial settings for pump components, wear housing, plates, conveyor wear parts, skids, and skid rails.

Another method for producing ausferrite in cast iron involves the modification of its chemical composition. This process is facilitated by the addition of molybdenum along with nickel or copper. Molybdenum plays a crucial role in altering the stability of austenite, enhancing its stability during pearlitic transformation while minimally affecting it during bainitic transformation. Consequently, in cast iron without Mo, continuous cooling in a mold leads to the pearlite transformation of austenite, whereas in molybdenum-containing cast iron, ausferrite transformation occurs. To prevent pearlite precipitation, nickel or copper are also introduced into the cast iron. Research on ausferrite obtained in cast iron without heat treatment has been conducted in various studies [24–26].

The primary objective of this paper is to compare the morphology of ausferrite obtained through heat treatment and in its raw state (as cast). Additionally, this study aims to investigate the influence of the chemical composition of as-cast ausferritic ductile cast iron on the carbon content in the austenite.

## 2. Materials and Methods

The cast iron used in this study was melted in an induction electric furnace with a crucible capacity of 30 kg (Elkon PI30, “ELKON” Ltd., Rybnik, Poland). The furnace charge

consisted of special pig iron (with a sulfur of less than 0.01%), ferrosilicon, ferromanganese, and technically pure Mo, Cu, and Ni. The chemical composition of the tested cast iron is presented in Table 4.

**Table 4.** The chemical composition of the tested cast iron.

Cast Iron Designation *	Chemical Composition, wt. %							
	C	Si	Mn	P	S	Mo	Cu	Ni
ADI	3.41	2.62	0.30	0.046	0.016	-	0.46	-
Cu ADCI	3.44	2.44	0.33	0.050	0.023	1.51	1.96	-
Ni ADCI	3.57	2.39	0.32	0.065	0.015	1.77		1.93

\* ADI—ausferritic ductile cast iron after heat treatment; Cu ADCI—as-cast ausferritic ductile cast iron with Cu; Ni ADCI—as-cast ausferritic ductile cast iron with Ni.

The magnesium treatment was conducted using the Inmold technology, which entails situating the master alloy in a gating system within a reaction chamber. The chemical composition of the master alloy is detailed in Table 5.

**Table 5.** The chemical composition of the master alloy.

Chemical Composition, wt. %					
Si	Mg	Ca	La	Al	Fe
44–48	5–6	0.4–0.6	0.25–0.40	0.8–1.2	rest

Silicon in the master alloy functions as a graphite-forming element, while magnesium and lanthanum facilitate the attainment of a spheroidal graphite shape. Aluminum and calcium act as inoculants, refining the microstructure components.

Following the smelting of the charge, it was superheated to 1530 °C. Subsequently, the cast iron was poured into a mold, flowing through the pouring cup and sprue into the reaction chamber where it mixed with the master alloy. In the mixing chamber, the remaining master alloy was dissolved. A control chamber enabled the measurement of the cast iron temperature, with a PtRh10-Pt thermocouple placed in the thermal center of the control chamber. This thermocouple was connected to compensation wires, transmitting the voltage signal to the Cristaldigraph 8T (voltage-frequency converter) by “Z-Tech”, Gliwice, Poland, and then to a computer equipped with software for recording thermal and derivative analysis (TDA) curves.

The test casting featured a stepped shape with wall thicknesses of 3, 6, 12, and 24 mm. After cooling to approximately 200 °C, the casting was removed from the mold and allowed to cool to ambient temperature. Test specimens were extracted from each of the four center sections of the stepped casting. For ADI, the casting underwent a heat treatment involving austenitizing at 900 °C for 1 h, followed by cooling in a salt bath and isothermal holding at 400 °C for 2 h. The salt bath for isothermal holding comprised sodium and potassium nitrate (NaNO<sub>3</sub> + KNO<sub>3</sub>) in a 50%:50% ratio, a process known as austempering, ensuring the formation of an ausferritic microstructure.

To examine the microstructures of the tested cast iron, quantify the content of austenite and ferrite in the microstructure, and qualitatively assess the primary graphite shape, metallographic sections were prepared. The specimens were ground using sandpapers ranging from 180 to 1200 grit, polished with 1 µm and 3 µm diamond suspensions, and finally polished with a 0.05 µm colloidal suspension. The unetched cross-sections were observed using a JEOL JESM 6610LV scanning microscope (JEOL, 3-1-2 Musashino, Akishima, Tokyo) equipped with backscattered electron diffraction capabilities from Oxford Instruments (Oxford Instruments NanoAnalysis, UK, Halifax Road, High Wycombe Buckinghamshire). Microstructure images were captured at magnification of ×100 and ×800, with EBSD tests conducted on the prepared surfaces. For EBSD mapping, an accelerating voltage of 20 kV

and a step size of 0.33  $\mu\text{m}$  were employed. To determine the concentration of austenite by XRD in the examined cast irons, a PROTO iXRD diffractometer with a position-sensitive detector (Proto Manufacturing Ltd., LaSalle, ON, Canada) was utilized. The X-ray source was a Cr anode tube operating at 20 kV and 4 mA, emitting characteristic radiation with a wavelength of  $\lambda = 2.29 \text{ \AA}$ . The irradiation was limited by a 2 mm diameter mask. The instrument collected four diffraction peaks, two for the ferrite/martensite phase, (200) planes and (211) planes positioned at  $106^\circ$  and  $156^\circ$   $2\theta$ , respectively, and two for the austenite phase— $79^\circ$  for (200) and  $128^\circ$  for (220) planes. The volume percent concentration of retained austenite was determined by comparing the intensities of these peaks following ASTM E-975 standard procedures [27].

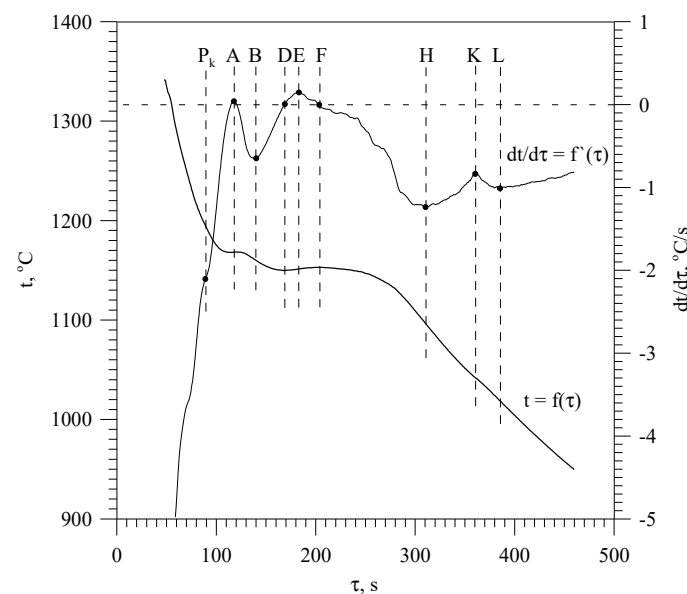
The carbon content calculations in austenite were conducted using Thermo-Calc 2018b (Thermo-Calc Software AB, Solna, Sweden). These calculations were specifically performed for cast iron without heat treatment.

### 3. Results and Discussion

#### 3.1. Thermal and Derivative Analysis Curves

In as-cast ausferritic ductile cast iron, the final properties are obtained after the casting has finished cooling in the mold. Accordingly, Figure 1 shows the thermal and derivative analysis (TDA) curves of as-cast ausferritic ductile cast iron containing approximately 1.5% Mo and 2% Cu (Cu ADCI).

On the derivative curve (also known as the crystallization curve)  $dt/d\tau = f'(\tau)$ , various thermal effects are described by characteristic points. The PkAB thermal effect arises from the transformation of liquid into primary austenite. The transformation of the liquid into a eutectic mixture of nodular graphite and austenite results in the DEFH thermal effect. Due to the simple microsegregation of molybdenum, the liquid becomes significantly enriched in Mo towards the end of crystallization, leading to its crystallization following a metastable system. Consequently, the HKL thermal effect stems from the crystallization of ledeburitic carbides. The crystallization process of cast iron concludes at  $1019^\circ\text{C}$  (point L).



Point	$\tau, \text{ s}$	$t, ^\circ\text{C}$	$dt/d\tau, ^\circ\text{C/s}$
P <sub>k</sub>	89	1195	-2.11
A	118	1168	0.04
B	140	1160	-0.65

Figure 1. Cont.

D	169	1150	-
E	183	1151	0.16
F	204	1153	-
H	310	1097	-1.24
K	360	1042	-0.84
L	385	1019	-1.01

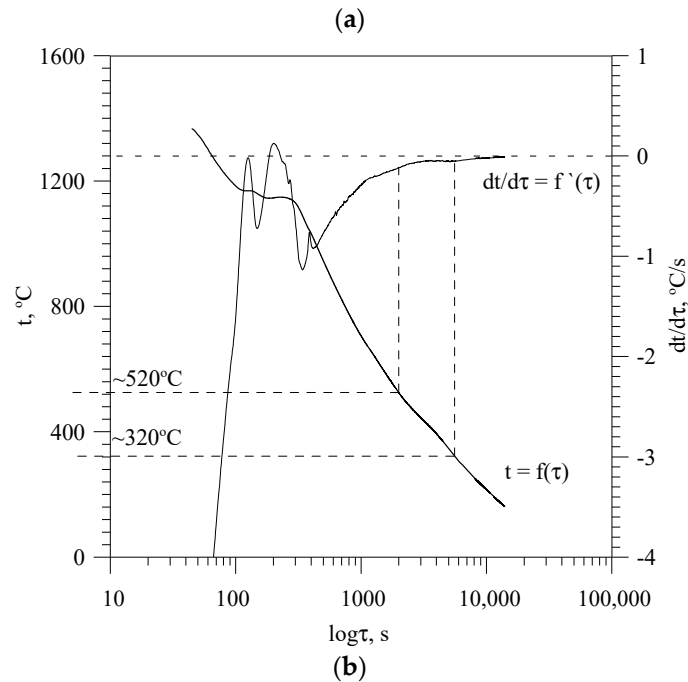
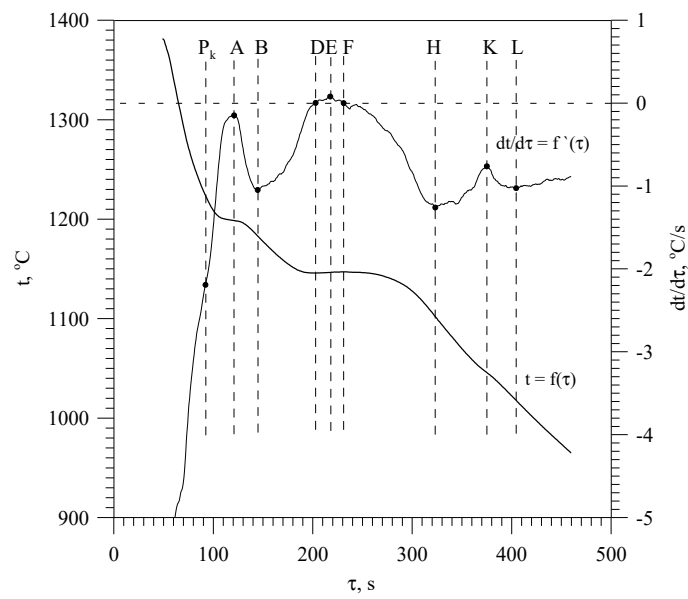


**Figure 1.** (a,b) TDA curves with descriptions of the characteristic points of as-cast ausferritic ductile cast iron containing approximately 1.5% Mo and 2% Cu (Cu ADCI) in the region of crystallization (a) and crystallization with solid-state transformation (b).

In Figure 1b, the TDA curves of cast iron are depicted in both the crystallization and solid-state transformation areas. The austenite transformation can be seen as a minor thermal effect within the temperature range of approximately 520–320 °C ( $\pm 10$  °C). The initiation and termination of this transformation were approximated by deviating from the so-called calorimetric curve, which represents the derivative curve devoid of thermal effects. Mathematically, the onset of the thermal effect from the transformation of austenite into bainitic ferrite (for both copper and nickel cast iron) corresponds to the inflection point of the derivative curve, while its end is the local minimum. The two points described above were determined using a graphical method. It should be noted that precise determination of the initiation and termination of this effect is not feasible due to the disturbances during the recording of the curves and the slight amount of heat released during the transformation of austenite to bainitic ferrite. This effect arises from the transformation of austenite into bainitic ferrite, resulting in the formation of ausferrite (a blend of bainitic ferrite and austenite) within the cast iron matrix.

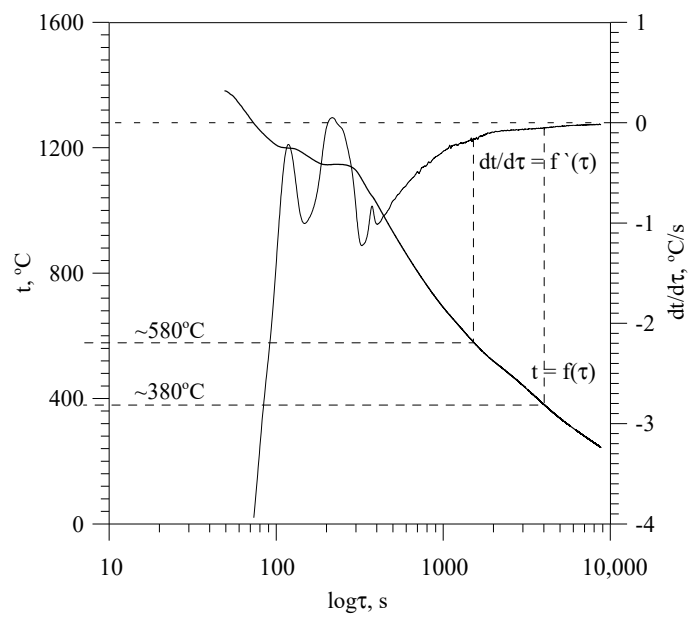
This research demonstrates that through the addition of molybdenum and copper in ductile cast iron, it is feasible to achieve ausferrite in its raw state without to need for casting heat treatment. This absence of a thermal effect from the eutectoid transformation, involving the conversion of austenite into a mixture of ferrite and cementite (pearlite), is evident on the derivative curve  $dt/d\tau = f'(\tau)$ .

Figure 2 displays TDA curves of as-cast ausferritic ductile cast iron containing approximately 1.7% Mo and 2% Ni (Ni ADCI).



Point	$\tau, s$	$t, ^\circ C$	$dt/d\tau, ^\circ C/s$
P <sub>k</sub>	71	1215	-1.91
A	104	1186	-0.06
B	135	1173	-0.71
D	197	1145	-
E	209	1146	0.20
F	242	1150	-
H	347	1094	-1.18
K	395	1046	-0.77
L	431	1015	-0.92

(a)



(b)

**Figure 2.** (a,b) TDA curves with descriptions of the characteristic points of as-cast ausferritic ductile cast iron containing approximately 1.7% Mo and 2% Ni (Ni ADCI) in the region of crystallization (a) and crystallization with solid-state transformation (b).

The crystallization process of as-cast ausferritic ductile cast iron containing approximately 1.7% Mo and 2% Ni, as depicted in Figure 2a, unfolds similarly to that of cast iron containing copper (Figure 1a). At a comparable molybdenum concentration, the eutectic transformation in both stable (DEFH thermal effect) and metastable (HKL thermal effect) systems occurs at a temperature approximately 3–4 °C lower than in cast iron containing about 2% Cu. Moreover, there was no significant impact of nickel on the temperature of eutectic transformation in the stable system. However, nickel was observed to elevate the temperature of the end of carbide crystallization (point L, Figure 2a) by roughly 5 °C per 1% Ni. A notable variation was noted in the realm of austenite transformation, which, for Ni ADCI, takes place within the temperature range of about 580–380 °C ( $\pm 10$  °C) (Figure 2b), i.e., approximately 60 °C higher than for cast iron with copper (Cu ADCI). The methodology for its determination was analogous to that for cast iron with copper. Similarly to the previously described cast iron, it was shown that through the common addition of molybdenum and nickel in ductile cast iron, it is feasible to obtain ausferrite in the raw state (as cast).

### 3.2. Scanning Electron Microscope Images

The Scanning Electron Microscope (SEM) images of the unetched microstructure of the tested cast irons are presented in Figure 3a–f.

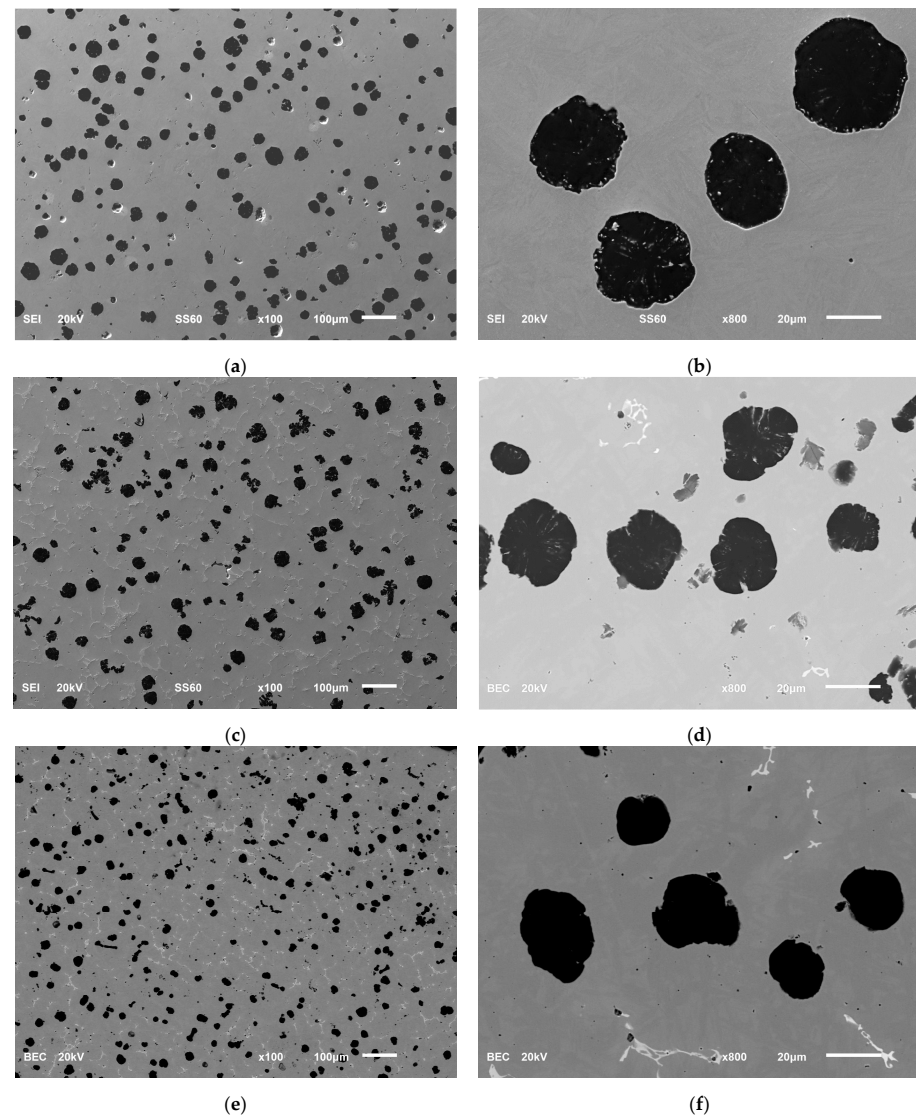


**Figure 3.** (a–f) Unetched cast iron microstructure. (a) ADI magn.  $\times 100$ , (b) ADI, magnification  $\times 800$ , (c) Cu ADCI, magnification  $\times 100$ , (d) Cu ADCI magn.  $\times 800$ , (e) Ni ADCI, magn.  $\times 100$ , (f) Ni ADCI, magn.  $\times 800$ .

From the data presented in Figure 3a–f, it is evident that the microstructure of the tested cast iron primarily comprises nodular graphite (classified as No. VI according to EN ISO 945-1:2019-09). In ausferritic cast iron obtained without heat treatment (depicted in Figure 3c–f), deformed nodular graphite (No. V) and compacted (vermicular) graphite (No. III) are also observed. This occurrence can be attributed to the inclusion of molybdenum, which impedes the crystallization of nodular graphite. Additionally, the microstructure in the matrix reveals a minor presence of carbides along the eutectic grain boundaries, a consequence of molybdenum's carbide-forming characteristics.

It is crucial to highlight that the presence of compacted graphite may diminish the strength properties of as-cast ausferritic ductile iron. Considering the existence of carbides, it can be inferred that Ni ADCI and Cu ADCI are likely to exhibit higher hardness and enhanced wear resistance compared to ADI.

### 3.3. Electron Backscatter Diffraction Results and X-ray Diffraction Austenite Content

The Electron Backscatter Diffraction (EBSD) tests facilitated the evaluation of the microstructure of the matrix composed of austenite and ferrite, enabling the determination of the proportions of these phases. Figure 4a–f showcases images of band contrast (BC) and phase distribution in the examined areas. Tables 4–6 provide qualitative results of phase content measured by EBSD and austenite contents measured by X-ray Diffraction (XRD). These tables also furnish details on the Mean Angular Deviation, which signifies the degree of the solution. A lower MAD value indicates a better alignment between the detected Kikuchi bands and the simulation, with a value below  $1^\circ$  generally considered acceptable for most systems.

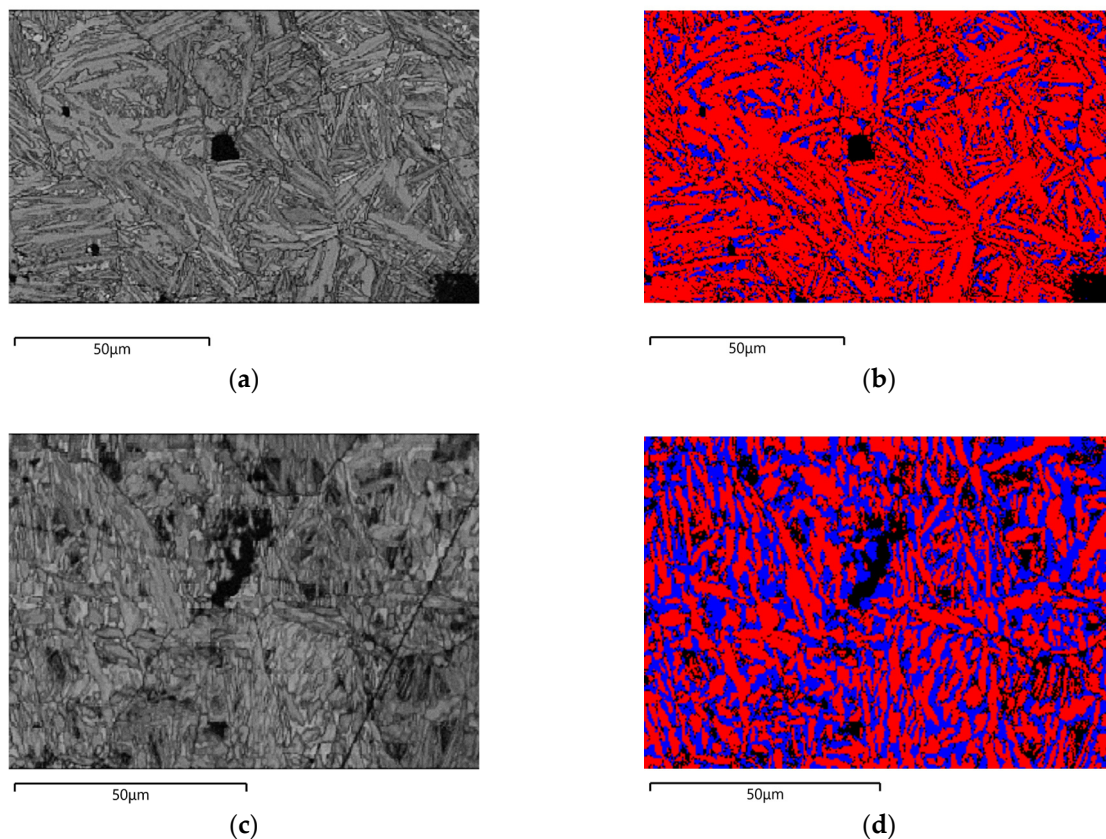
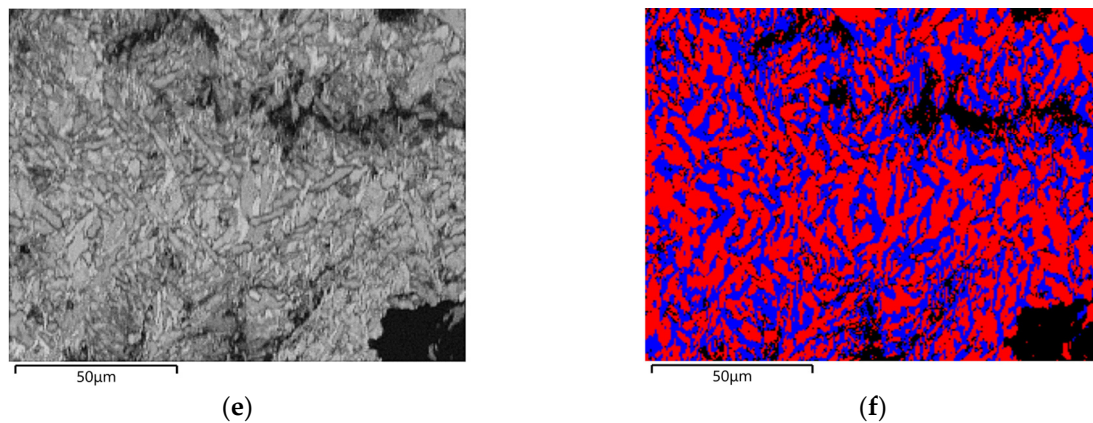


Figure 4. Cont.



**Figure 4.** (a–f) Images of band contrast and phase distribution in examined areas of cast irons. Blue areas represent the Fe-FCC (austenite) phase and red Fe-BCC (ferrite), (a) ADI band contrast, (b) ADI phase distribution, (c) Cu ADCI band contrast, (d) Cu ADCI phase distribution, (e) Ni ADCI band contrast, and (f) Ni ADCI phase distribution. The black areas, the unindexed parts of the structures, are the precipitations of graphite, molybdenum carbides, or surface discontinuities.

**Table 6.** Phase content, MAD parameter, and XRD austenite content for the tested cast iron.

Type of Cast Iron	Phase Name	Phase Fraction, wt. %	Mean MAD	Standard Deviation MAD	XRD, wt. %
ADI	Fe-BCC	84.71	0.7653	0.3530	-
	Fe-FCC	13.75	0.7695	0.3600	18.4 ± 1.7
	Zero Solutions	1.54	-	-	-
Cu ADCI	Fe-BCC	55.54	0.7385	0.3156	-
	Fe-FCC	41.51	0.7391	0.3451	40.7 ± 3.2
	Zero Solutions	2.95	-	-	-
Ni ADCI	Fe-BCC	54.63	0.4746	0.2855	-
	Fe-FCC	39.59	0.4269	0.2880	36.5 ± 2.2
	Zero Solutions	5.78	-	-	-

The data in Figure 4 indicate that the structure of bainitic ferrite platelets in ADI (Figure 4a) closely resembles that in as-cast ausferritic ductile cast iron (Figure 4c,f). Figure 4a–f and Table 6 reveal that the austenite content in the matrix is the lowest for ADI, approximately 14%, when assessed via the EBSD method, while it measures around 18% using XRD. This discrepancy arises from the presence of dark areas that were not identified through the EBSD method. In contrast, for as-cast ausferritic ductile cast iron with Ni and Cu (Ni ADCI and Cu ADCI), the austenite content was notably higher, at about 40% and 41%, respectively. This higher austenite content is attributed to the presence of nickel and copper, recognized as austenite-forming elements. The elevated austenite content may enhance the strength properties, as it undergoes a martensitic-type transformation during operation through the microtwinning mechanism under unit pressures. As a result, machine and equipment components crafted from such cast iron are expected to exhibit high resistance to abrasive wear.

### 3.4. Carbon Content in an Austenite

The investigated cast iron with an ausferritic microstructure demonstrates significant resistance to abrasive wear. In general, the wear resistance of cast iron depends mainly on the qualitative and quantitative proportion of phases in its microstructure, including ferrite, austenite, carbides, and graphite.

In conventional unalloyed cast iron, which crystallizes under near-equilibrium conditions, graphite and/or ledeburite (a mixture of austenite and cementite) form during the

eutectic transformation. If the eutectic transformation occurs partially in the metastable system, carbides can be segregated from austenite due to varying carbon solubility. As per the Fe-Fe<sub>3</sub>C equilibrium phase diagram, most carbides precipitate as cementite (Fe<sub>3</sub>C) within the range between eutectic and eutectoid temperatures, known as secondary carbides. During eutectoid transformation, austenite is transformed into pearlite, a mixture of ferrite and cementite. The carbon solubility in ferrite is significantly lower compared to that in austenite, leading to negligible formation of tertiary carbides due to varying carbon solubility in ferrite. Thus, the wear resistance of near-equilibrium cast iron is dictated by the quantity of precipitated secondary carbides, contingent on the maximum carbon dissolved in austenite. In contrast, the cast irons discussed in this study exhibit distinct characteristics. In this case, there is no eutectoid transformation and no pearlite formation, and thus no carbides contained in the form of cementite. The presence of alloying elements alters the carbon solubility ranges in austenite, with molybdenum acting as a carbide-forming element by bonding a portion of the carbon. Consequently, the carbide content differs from that predicted by the Fe-Fe<sub>3</sub>C phase diagram. The cast irons under investigation possess an ausferritic matrix at ambient temperature, comprising austenitic–ferritic phases. Therefore, carbon dissolved in austenite does not contribute to carbide formation. Additionally, the substantial silicon content in the cast iron (approximately 2.5%) acts as a graphite-forming element and impedes carbide formation. Carbides may form due to the decreasing carbon solubility in austenite within the temperature range from eutectic to eutectoid, coupled with the partially diffusionless transformation of austenite into bainitic ferrite. Consequently, the carbide content and wear resistance of cast iron are influenced by the proportions of ferrite and austenite in the matrix. A lower austenite content leads to excess carbon and increased carbide formation.

The carbon content dissolved in austenite at eutectic and eutectoid temperatures also plays a role in carbide formation. Higher dissolved carbon at the eutectic temperature and lower at the eutectoid temperature result in more carbides. The carbon content in austenite also impacts its mechanical properties, with higher dissolved carbon enhancing them. Understanding these solubilities is crucial for determining the properties of austenite. It is noteworthy that in the examined cast iron, austenite can undergo a diffusionless transformation via the microtwinning mechanism, reinforcing the matrix and enhancing wear resistance. Higher carbon concentrations in the cast iron matrix lead to elevated mechanical properties akin to martensite. However, comprehensive data on these solubilities are lacking in the available literature, especially considering that any alterations in chemical composition can affect these solubilities. Table 7 outlines the carbon solubility in austenite for the tested as-cast ausferritic ductile cast iron.

**Table 7.** Carbon solubility in an austenite for the tested as-cast ausferritic ductile cast iron.

Type of Cast Iron	Type of Transformation	Transformation Temperature, °C	Carbon Solubility, wt. %
Ni ADCI	Eutectic	1118	1.38
	Eutectoid	784	0.49
Cu ADCI	Eutectic	1133	1.44
	Eutectoid	783	0.47

From the data provided in Table 7, it is evident that the analyzed cast irons exhibit a restricted range of austenite stability compared to the conventional Fe-Fe<sub>3</sub>C system, leading to decreased carbon solubility in austenite at both eutectic and eutectoid temperatures. Nevertheless, there are no significant disparities in solubility between the two cast irons. Given the impracticality of determining the carbon content in austenite experimentally, this article assumes the carbon levels based on the phase equilibrium diagrams generated by the program.

#### 4. Conclusions

This study showcases the feasibility of achieving ausferrite in ductile cast iron without the need for heat treatment through the addition of molybdenum in conjunction with nickel or copper. The morphology of bainitic ferrite platelets closely resembles that of ADI.

The thermal and derivative analysis (TDA) curves revealed a heating effect attributed to the transformation of austenite into bainitic ferrite in as-cast ausferritic ductile cast iron, with the temperature range being approximately 60 °C higher for nickel cast iron.

Scanning Electron Microscope (SEM) imaging unveiled that the introduction of alloying elements induced distortions in nodular graphite growth, leading to its deformation and the formation of slightly irregular or even compacted graphite (classified as type V and III according to EN ISO 945-1:2019-09). Electron Backscatter Diffraction (EBSD) analysis demonstrated that the matrices of the tested irons comprise fine acicular structures containing both austenite and ferrite. In the case of Cu ADCI and Ni ADCI, the austenite content is notably higher than in ADI, a finding corroborated by XRD measurements, indicating structural uniformity despite differences in the volumes used for calculating austenite content in both methods. While a hit rate exceeding 95% is considered very good, Mean Angular Deviation (MAD) values, generally falling within an acceptable range, may suggest distortions in Kikuchi lines positions and widths, indicative of high stress in both austenite and ferrite phases. The findings presented in this article can aid in material selection for machine components prone to abrasive and adhesive wear. As-cast ductile cast iron, being more cost-effective to produce, can serve as a viable alternative to ADI.

**Author Contributions:** Conceptualization, G.G. and L.K.; methodology, G.G., B.J. and L.K.; software, B.J. and R.A.; validation, G.G., L.K. and B.J.; formal analysis, G.G. and L.K.; investigation, B.J. and R.A.; resources, G.G.; data curation, B.J.; writing—original draft preparation, G.G., L.K. and B.J.; writing—review and editing, L.K. and G.G.; visualization, K.B.; supervision, G.G., L.K. and K.B.; project administration, K.B.; funding acquisition, G.G. All authors have read and agreed to the published version of the manuscript.

**Funding:** This research was funded by the Institutional Endowment for the Long-Term Conceptual Development of Research Institutes, as provided by the Ministry of Education, Youth and Sports of the Czech Republic in the year 2024.

**Data Availability Statement:** The raw data supporting the conclusions of this article will be made available by the authors on request.

**Acknowledgments:** This publication was written at the Technical University of Liberec, Faculty of Mechanical Engineering, supported by the Institutional Endowment for the Long-Term Conceptual Development of Research Institutes, as provided by the Ministry of Education, Youth and Sports of the Czech Republic in the year 2024.

**Conflicts of Interest:** The authors declare no conflicts of interest.

#### References

1. EN ISO 945-1:2019-09; Microstructure of Cast Irons, Part 1: Graphite Classification by Visual Analysis. International Organization for Standardization: Geneva, Switzerland, 2019.
2. EN 1563:2018-10; Founding—Spheroidal Graphite Cast Irons. European Committee for Standardization: Brussels, Belgium, 2018.
3. Rundman, K.B.; Moore, D.J.; Hayrynen, K.L.; Dubensky, W.J.; Rouns, T.N. The Microstructure and Mechanical Properties of Austempered Ductile Iron. *J. Heat Treat.* **1988**, *5*, 79–95. [[CrossRef](#)]
4. Górny, M.; Gondek, Ł.; Tyrała, E.; Angella, G.; Kawalec, M. Structure homogeneity and thermal stability of austempered ductile iron. *Metall. Mater. Trans. A* **2021**, *52*, 2227–2237. [[CrossRef](#)]
5. Górny, M.; Angella, G.; Tyrała, E.; Kawalec, M.; Paž, S.; Kmita, A. Role of austenitization temperature on structure homogeneity and transformation kinetics in austempered ductile iron. *Met. Mater. Int.* **2019**, *25*, 956–965. [[CrossRef](#)]
6. Wang, C.; Du, X.; Li, S.; Sun, Y.; Yang, P. Morphology and crystallography of ausferrite in austempered ductile iron. *Metals* **2017**, *7*, 238. [[CrossRef](#)]
7. Skudlarek, W.; Krmasha, M.N.; Al-Rubaie, K.S.; Preti, O.; Milan, J.C.; da Costa, C.E. Effect of austempering temperature on microstructure and mechanical properties of ductile cast iron modified by niobium. *J. Mater. Res. Technol.* **2021**, *12*, 2414–2425. [[CrossRef](#)]

8. Yang, P.; Fu, H.; Absi, R.; Bennacer, R.; Darcherif, M.; Ma, S.; Lin, J.; Guo, X. Microstructure evolution of carbidic austempered ductile iron at different austempering temperatures. *J. Mater. Sci.* **2021**, *56*, 4843–4857. [[CrossRef](#)]
9. Hegde, A.; Sharma, S.; Hande, R.; Gurumurthy, B.M. Microstructure and Mechanical Properties of Manganese-Alloyed Austempered Ductile Iron Produced by Novel Modified Austempering Process. *Cogent Eng.* **2022**, *9*, 2046301. [[CrossRef](#)]
10. Mussa, A.; Krakhmalev, P.; Bergström, J. Wear Mechanisms and Wear Resistance of Austempered Ductile Iron in Reciprocal Sliding Contact. *Wear* **2022**, *498*, 204305. [[CrossRef](#)]
11. Tuan, H.A.; Hai, N.H.; Dung, N.H.; Nam, N.D. Austenitization and Formation of Ausferrite Structure in Austempered Ductile Iron with Dual Matrix. *Mater. Res. Express* **2022**, *9*, 046520. [[CrossRef](#)]
12. Raghavendran, R.; Meena, A. Deformation Induced Microstructure Evolution and Phase Transformation in an Austempered Ductile Iron (ADI). *Int. J. Met.* **2023**, *17*, 233–247. [[CrossRef](#)]
13. Liu, C.; Du, Y.; Wang, X.; Zheng, Q.; Zhu, X.; Zhang, D.; Liu, D.; Yang, C.; Jiang, B. Comparison of the tribological behavior of quench-tempered ductile iron and austempered ductile iron with similar hardness. *Wear* **2023**, *520*, 204668. [[CrossRef](#)]
14. Jaśkowiec, K.; Opaliński, A.; Kustra, P.; Jach, D.; Wilk-Kołodziejczyk, D. Prediction of Selected Mechanical Properties in Austempered Ductile Iron with Different Wall Thickness by the Decision Support Systems. *Arch. Foundry Eng.* **2023**, *23*, 137–144. [[CrossRef](#)]
15. Górný, M.; Gondek, Ł.; Angella, G.; Tyrała, E.; Kawalec, M.; Bitka, A. Structural Stability of Thin-Walled Austempered Ductile Iron Castings. *Arch. Civ. Mech. Eng.* **2023**, *23*, 79. [[CrossRef](#)]
16. Uyar, A.; Sahin, O.; Nalcaci, B.; Kilicli, V. Effect of Austempering Times on the Microstructures and Mechanical Properties of Dual-Matrix Structure Austempered Ductile Iron (DMS-ADI). *Int. J. Met.* **2022**, *16*, 407–418. [[CrossRef](#)]
17. Angella, G.; Donnini, R.; Ripamonti, D.; Bonollo, F.; Cygan, B.; Gorný, M. On Ausferrite Produced in Thin Sections: Stability Assessment through Round and Flat Tensile Specimen Testing. *Metals* **2023**, *13*, 105. [[CrossRef](#)]
18. Keleş, A.; Cengiz, R.; Yildirim, M. Effect of Alloying Elements and Technological Parameters of Austempering on the Structure and Mechanical Properties of Ductile Cast Iron (ADI). *Met. Sci. Heat Treat.* **2023**, *65*, 191–199. [[CrossRef](#)]
19. EN 1564:2012; Founding—Ausferritic Spheroidal Graphite Cast Irons. European Committee for Standardization: Brussels, Belgium, 2012.
20. Batra, U.; Singh, M.; Sharma, S.K. Effect of austempering temperature on microstructure and tribological behaviour of hypoeutectic austempered ductile iron alloyed with copper. *Tribol.-Mater. Surf. Interfaces* **2022**, *16*, 342–355. [[CrossRef](#)]
21. Nofal, A. Advances in the Metallurgy and Applications of ADI. *J. Metall. Eng.* **2013**, *2*, 84.
22. Sharun, V.; Ronald, B.A. Traditional Machining of Austempered Ductile Iron (ADI): A Review. *Mater. Today Proc.* **2023**, *72*, 2027–2031. [[CrossRef](#)]
23. Wang, B.; Qiu, F.; Barber, G.C.; Pan, Y.; Cui, W.; Wang, R. Microstructure, Wear Behavior and Surface Hardening of Austempered Ductile Iron. *J. Mater. Res. Technol.* **2020**, *9*, 9838–9855. [[CrossRef](#)]
24. Tenaglia, N.E.; Pedro, D.I.; Boeri, R.E.; Basso, A.D. Influence of Silicon Content on Mechanical Properties of IADI Obtained From as cast Microstructures. *International J. Cast Met. Res.* **2020**, *33*, 72–79. [[CrossRef](#)]
25. de la Torre, U.; González-Martínez, R.; Méndez, S. Effect of the Section Size, Holding Temperature and Time on the Kinetics of the Ausferritic Transformation and Mechanical Properties of As-Cast Ausferritic Ductile Iron. *Mater. Sci. Eng. A* **2020**, *788*, 139536. [[CrossRef](#)]
26. Ferry, M.; Xu, W. Microstructural and crystallographic features of ausferrite in as-cast gray iron. *Mater. Charact.* **2004**, *53*, 43–49. [[CrossRef](#)]
27. E975-03; Standard Practice for X-ray Determination of Retained Austenite in Steel with Near Random Crystallographic Orientation. ASTM International: West Conshohocken, PA, USA, 2008.

**Disclaimer/Publisher’s Note:** The statements, opinions and data contained in all publications are solely those of the individual author(s) and contributor(s) and not of MDPI and/or the editor(s). MDPI and/or the editor(s) disclaim responsibility for any injury to people or property resulting from any ideas, methods, instructions or products referred to in the content.